LETTER

doi:10.1038/nature13260

Tropical forcing of the recent rapid Arctic warming in northeastern Canada and Greenland

Qinghua Ding[1], John M. Wallace[2], David S. Battisti[2], Eric J. Steig[1], Ailie J. E. Gallant[3], Hyung-Jin Kim[4] & Lei Geng[2]

Rapid Arctic warming and sea-ice reduction in the Arctic Ocean are widely attributed to anthropogenic climate change[1–3]. The Arctic warming exceeds the global average warming because of feedbacks that include sea-ice reduction[4,5] and other dynamical and radiative feedbacks[6–13]. We find that the most prominent annual mean surface and tropospheric warming in the Arctic since 1979 has occurred in northeastern Canada and Greenland. In this region, much of the year-to-year temperature variability is associated with the leading mode of large-scale circulation variability in the North Atlantic, namely, the North Atlantic Oscillation[14,15]. Here we show that the recent warming in this region is strongly associated with a negative trend in the North Atlantic Oscillation, which is a response to anomalous Rossby wave-train activity originating in the tropical Pacific. Atmospheric model experiments forced by prescribed tropical sea surface temperatures simulate the observed circulation changes and associated tropospheric and surface warming over northeastern Canada and Greenland. Experiments from the Coupled Model Intercomparison Project Phase 5 (ref. 16) models with prescribed anthropogenic forcing show no similar circulation changes related to the North Atlantic Oscillation or associated tropospheric warming. This suggests that a substantial portion of recent warming in the northeastern Canada and Greenland sector of the Arctic arises from unforced natural variability.

The recent Fifth Assessment Report of the Intergovernmental Panel on Climate Change[1] anticipates the continuing retreat of sea ice and warming accompanying future anthropogenic emissions of greenhouse gases and aerosols. However, natural variability, such as that associated with the Atlantic Multi-decadal Oscillation[6], has been suggested to be an important driver of climate variations in the Arctic region and responsible for a portion of the recent warming trend. Some recent results also indicate that sea surface temperature (SST) changes outside the Arctic have played a role in forcing the recent tropospheric warming in the Arctic[17].

In this study, we use observational analyses and modelling to explore the relative contributions of anthropogenic forcing and natural variability to recent warming trends in the Arctic. We identify a specific tropical SST pattern that has contributed significantly to recent Arctic warming by changing the circulation over northern high latitudes.

We use post-1979 observations only, because the analyses of geopotential height (which approximates the actual height of a pressure surface above mean sea level) and other variables over the Northern Hemisphere polar region are more reliable during the modern satellite era[18]. The most reliable reanalysis data sets (ERA-interim[19] and MERRA[20]) and station data[21,22] agree that the most pronounced annual mean surface temperature warming in the Arctic since 1979 has occurred over northeastern Canada, Greenland and the north of Siberia (Fig. 1a and Extended Data Fig. 1). Surface temperatures along the Siberian coast are highly negatively correlated ($r \approx -0.7$ to -0.9) with *in situ* sea-ice variability where the observed surface warming is greatest and can be related directly to the significant sea-ice reduction. The troposphere has also experienced an annual averaged warming in the Arctic. Tropospheric warming is most pronounced over northeastern Canada and Greenland, where it extends through the depth of the troposphere and has occurred in all seasons, with the largest magnitude and extent during boreal winter (December–February) (Fig. 1b, Extended Data Figs 2 and 3). The magnitude of the surface and tropospheric warming in the northeastern Canadian-Greenland sector of the Arctic is nearly twice as large as the Arctic-mean warming.

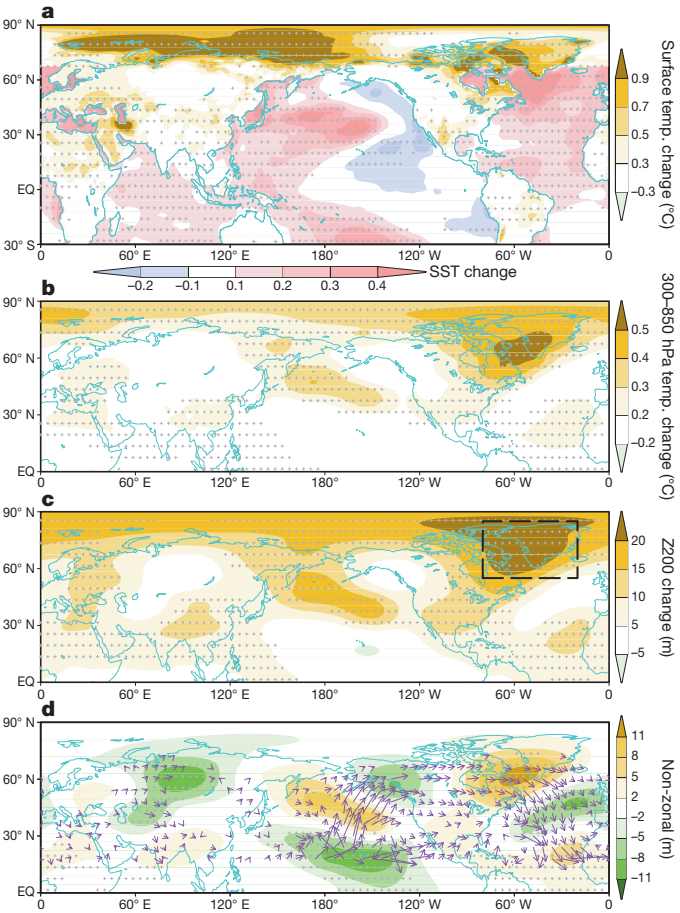

Figure 1 | Observed trend pattern of annual mean field for 1979–2012. Linear trend (per decade) of annual mean surface temperature (**a**), 300–850 hPa temperature (**b**), 200-hPa geopotential height (Z200; **c**) and the non-zonal component of 200-hPa geopotential height (**d**). In **a**, surface temperature is shown over land or ice; SST is shown over ocean. In **d**, purple vectors (units: 10^6 Pa m^2 s^{-2}, vectors less than 10^5 Pa m^2 s^{-2} are omitted) denote the wave activity flux associated with the eddy Z200 trend pattern. Grid points with trends that are statistically significant at the 99% confidence level are denoted by small crosses. The box in **c** indicates the domain over which data are averaged in Extended Data Fig. 6. EQ, Equator.

[1]Department of Earth and Space Sciences and Quaternary Research Center, University of Washington, Seattle, Washington 98195, USA. [2]Department of Atmospheric Sciences, University of Washington, Seattle, Washington 98195, USA. [3]School of Geography and Environmental Science, Monash University, Victoria 3800, Australia. [4]Climate Research Department, APEC Climate Center, 12 Centum 7-ro, Haeundae-gu, Busan 612-020, South Korea.

The spatially varying character of warming trends over the Arctic region suggests a role for atmospheric circulation changes. Annual mean 200-hPa geopotential heights (Z200) in the upper troposphere have increased almost everywhere in the Northern Hemisphere polar region since 1979, with the greatest increases occurring over northeastern Canada and Greenland, coinciding with the greatest surface and tropospheric warming (Fig. 1c and Extended Data Fig. 4). Consistent with the local surface temperature trend, the positive trend in Z200 over northeastern Canada and Greenland has occurred in all seasons, and is largest during winter (Extended Data Fig. 5). The correlation (r) between 34-year annual mean Z200 and surface temperature in this region is 0.9, and it is 0.8 for the detrended component (Extended Data Fig. 6a). Both the Z200 and surface temperature time series exhibit decadal-scale variability superimposed on the long-term trend. In all seasons, the seasonal and decadal anomalies in Z200 are highly correlated with the surface temperature anomalies (Extended Data Fig. 6b–e).

Because the upper-level atmospheric circulation is relatively insensitive to anomalous surface warming in the polar regions[7,17], it seems unlikely that the decadal-scale variations in Z200 in the 34-year record could be forced by local variations in surface temperature. Theory and a myriad of modelling studies suggest that causality operates in the opposite direction: that is, that the changes in surface and tropospheric temperature are an adiabatic response to the changes in the upper-level circulation, which may have been remotely forced.

The circulation trend is marked by rising geopotential heights over Greenland and near-steady heights along ~50° N over the North Atlantic (Fig. 1c). The pattern can be characterized as a uniform increase in geopotential heights across the Arctic, combined with the negative polarity of the North Atlantic Oscillation (NAO). The NAO is the leading mode of circulation variability and the main driver of temperature variability and extreme winter weather events in the North Atlantic[14,15]. A year-round NAO index, given by the leading principal component of low-level geopotential height anomalies in the North Atlantic[14], exhibits a strong ($r = 0.7$) correlation with surface temperature and Z200 anomalies in northeastern Canada and Greenland (Extended Data Fig. 6a). The past three decades have been marked by a negative trend in the NAO index[23].

Further insight into the causes of the remarkable warming trend over Greenland and northeastern Canada is gained by examining the trends in the eddy component of Z200, obtained by removing the zonal average at each latitude from the trends (Fig. 1c). The results (Fig. 1d) strongly suggest that the 200-hPa geopotential height increases over northeastern Canada and Greenland are associated with a Rossby wave train that originates in the tropical Pacific. The corresponding flux of wave activity exhibits a distinctive arc-shaped trajectory, extending from the central tropical Pacific towards the Arctic and returning to the tropics via the Atlantic sector. Coincident with the pattern of trends in the warming and anomalous circulation, SSTs (and rainfall) have increased significantly at the 99% confidence level throughout the tropics except for the central and eastern Pacific where they have remained nearly constant or even decreased slightly, as shown in Fig. 1a (Extended Data Fig. 7a). Motivated by two earlier studies[24,25], we hypothesize that this pattern of SST change in the tropics has played a key role in forcing the extra-tropical wave train that has both warmed northeastern Canada and Greenland and induced the negative trend in the NAO in recent decades.

Our hypothesis that the trend towards higher geopotential heights over northeastern Canada and Greenland has occurred in response to trends in tropical SST is supported by maximum covariance analysis (MCA)[26]. Figure 2 shows the leading modes of co-variability between annual mean Northern Hemisphere Z200, and tropical SST for the period 1979–2012. The leading MCA mode explains 68% of the squared covariance between the hemispheric Z200 and tropical SST fields, and captures the typical El Niño/Southern Oscillation (ENSO) signature in SST and the related atmospheric teleconnection pattern over the Pacific and North American sectors, with their familiar sequence of year-to-year variability. The patterns associated with the second mode resemble the trend in tropical SST and the wave-train pattern of the Z200 trend (Fig. 1a, c). The second MCA mode explains 28% of the squared covariance. The time series associated with this mode are strongly correlated ($r = 0.91$) and both exhibit a pronounced upward trend over the 34-year record. The time series of the SST pattern in mode 2 is highly correlated with the surface temperature in northeastern Canada and Greenland and with the year-round NAO index (Extended Data Fig. 8). This mode is not merely a reflection of the trends in the two fields, because similar MCA results are obtained when the data are detrended before conducting the MCA calculation (Extended Data Fig. 9). Thus, the wave train that links the positive temperature trends in northeastern Canada and Greenland to the tropical SST anomalies characterizes both

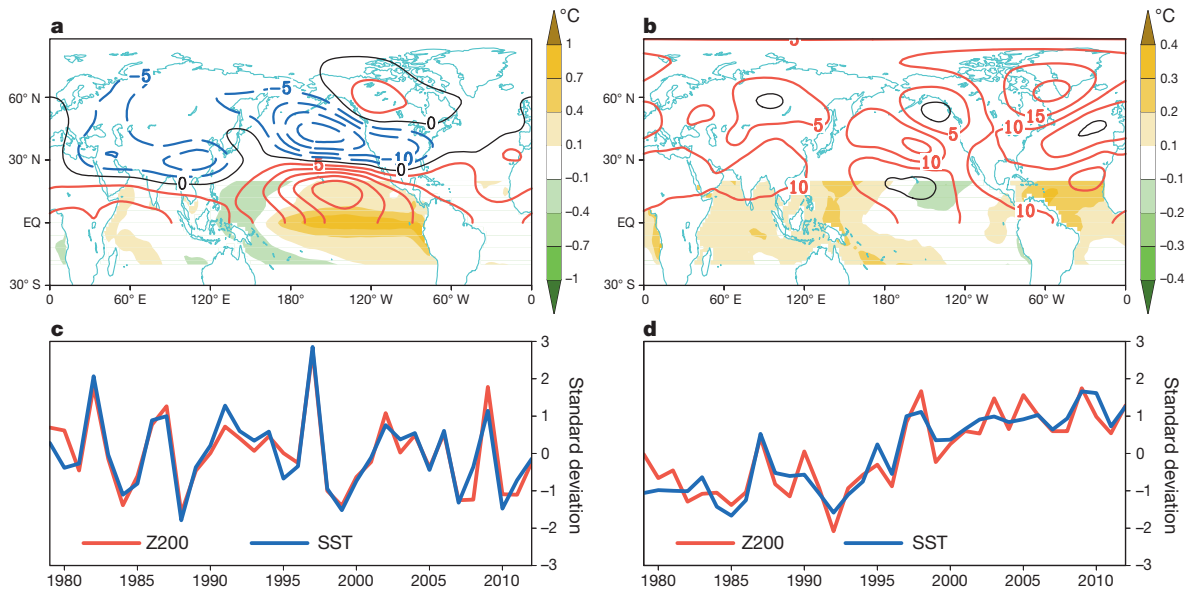

Figure 2 | Coupled patterns between annual mean tropical SST and Northern Hemisphere circulation for 1979–2012. a–d, Results of maximum covariance analysis for annual mean 1979–2012 Northern Hemisphere (0–88.5° N) 200-hPa geopotential height (Z200) and tropical (20° S to 20° N) SST. Shown in **a** are the patterns of Z200 (contours, interval 10 m) and tropical SST (shading; colour scale) that accompany the first mode. **c**, Time series of the Z200 (red) and SST (blue) patterns shown in **a**. Panels **b** and **d** are the same as panels **a** and **c**, but for the second mode. Amplitudes in **a** and **b** are scaled by one standard deviation of the corresponding time series in **c** and **d**.

interannual and interdecadal timescales. Compared to the circulation anomalies associated with typical ENSO, the circulation anomalies associated with the mode 2 pattern of SST anomalies exhibits a wave train that extends farther poleward and includes circulation anomalies over the North Atlantic that are very similar to those associated with the NAO. Thus, the recent 30-year trends in tropical SST—distinct from ENSO—may be partially responsible for the negative trend in the conventional NAO index.

To further examine the relationship between tropical SST forcing and circulation variability in northeastern Canada and Greenland, we use an atmospheric general circulation model (ECHAM 4.6 (ref. 27)) to perform an ensemble of integrations, each of which is forced by the observed tropical SST from 1979–2012; in the extratropics, the atmosphere is coupled to a slab ocean with a thermodynamic sea-ice component. Ten experiments were run, each with different initial atmospheric conditions, and averaging over the ten experiments is used to filter out intrinsic atmospheric variability. The ensemble-averaged change in the high-latitude circulation is, by construction, due to the remote tropical forcing and to the local amplification associated with sea-ice change. The ensemble-averaged trends in surface temperature, tropospheric temperature and Z200 in the Northern Hemisphere are shown in Fig. 3; in the western hemisphere they closely resemble the observed trends shown in Figs 1a–c, and are consistent with the trend patterns associated with the mode 2 in the MCA analysis. Rising 200-hPa heights and widespread warming over northeastern Canada and Greenland are an integral part of the response to the imposed tropical SST anomalies.

As in the observations, the simulated circulation anomaly over the North Atlantic is similar to that observed during the negative phase of the NAO. As in the observations, the warming trends and atmospheric circulation anomalies are largest in winter. The simulated annual mean Z200, surface and tropospheric temperature trends over northeastern Canada and Greenland are about 10 m per decade, 0.4 °C per decade and 0.3 °C per decade respectively, roughly half the magnitude of the values in the ERA-interim reanalysis[19]. We note that the model, forced by the observed tropical SST change, also reproduces the observed rainfall trend in the tropical Pacific (Extended Data Fig. 7b). The simulated wave-train path over the North Pacific and North Atlantic differs in detail from that observed (compare Figs 3d and 1d), possibly owing to subtle differences between the real and simulated climatological mean zonal flow. Nonetheless, the model results strongly suggest that a Rossby wave train associated with the observed tropical SST trend is responsible for the observed negative trend of the NAO and accounts for both the regional surface and tropospheric warming in northeastern Canada and Greenland.

Last, we explore the contribution of external forcing to the recent regional warming in northeastern Canada and Greenland. We take the ensemble-average response of the 40 climate models that were forced by historical forcing and archived in the CMIP5 database historical experiment[16]. We note that in these experiments, "historical forcing" includes both anthropogenic and natural forcing.

The trends in the ensemble-average surface and tropospheric temperature from the historical forcing simulations are shown in Fig. 4a and b. Comparing Fig. 1a to Fig. 4a, we see that the ensemble average of

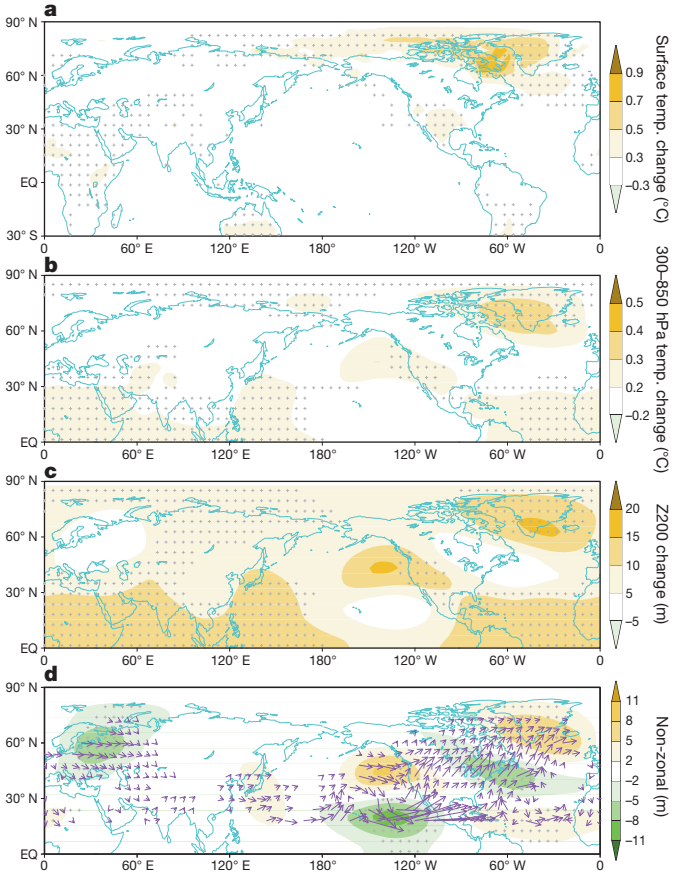

Figure 3 | Simulated 1979–2012 trend patterns in annual mean fields in ECHAM. Linear trend (per decade) of annual mean surface temperature (**a**), 300–850 hPa temperature (**b**), Northern Hemisphere 200-hPa geopotential height (Z200; **c**) and the non-zonal component of 200-hPa geopotential height from 34-year simulation of ECHAM run forced by observed SST (1979–2012) in the tropics (30° N to 30° S) (**d**). In the extratropics, the atmosphere is coupled to a slab ocean model. In **d**, purple vectors (units: 2.5×10^5 Pa m^2 s^{-2}, vectors less than 2.5×10^4 Pa m^2 s^{-2} are omitted) denote the wave activity flux associated with the eddy Z200 trend pattern. Grid points with trends that are statistically significant at the 99% confidence level are denoted by small crosses.

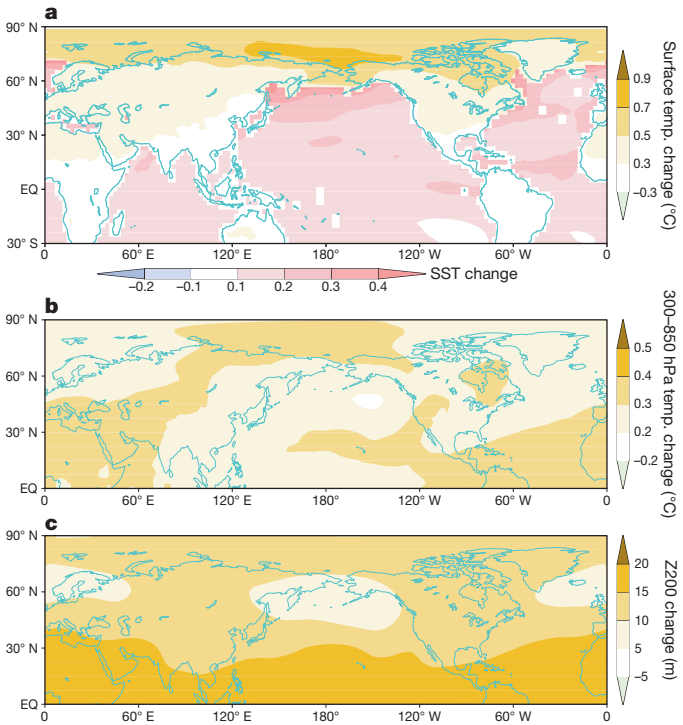

Figure 4 | Simulated 1979–2004 trend patterns in annual mean fields in CMIP5. Linear trend (per decade) of surface temperature (**a**), 300–850 hPa temperature (**b**) and 200-hPa geopotential height (Z200; **c**) for the period 1979–2004 due to anthropogenic and natural external forcing. Here we show the average of an ensemble of experiments using 40 climate models (Extended Data Table 1) that are archived in the CMIP5 database[16] and used in the Fifth Assessment Report of the Intergovernmental Panel on Climate Change[1]. The trends shown in the plot are significant at above the 99% confidence level at all grid points.

the historical simulations using the CMIP5 models shows a general warming throughout the globe—more so in the polar regions than in the tropics—with a maximum in the western Arctic Ocean due to reduced sea ice. The forced pattern of warming does not capture the cooling in the eastern tropical Pacific or the maximum warming over northeastern Canada and Greenland; in these regions, the CMIP5 models capture only about 40–50% of the observed warming in the surface and troposphere.

From a comparison of Figs 1c and 4c it is evident that the ensemble average of the historical simulations exhibits much larger Z200 rises in the tropics than observed, and slightly smaller increases in the polar region than observed. The most salient circulation feature in the observations is the pronounced localized rise in upper-tropospheric geopotential height and surface and tropospheric temperature over northeastern Canada and Greenland (Fig. 1). These features are not reproduced in the ensemble average of the historical simulations using the CMIP5 models.

The results from the ECHAM experiments forced by observed SST, together with the ensemble average of the historical simulations of the CMIP5 models, suggest that about half of the observed warming in northeastern Canada and Greenland is due to a uniform warming of the entire Arctic (directly attributable to anthropogenic forcing[1]); the other half is due to a wave train of circulation anomalies that extends from the central tropical Pacific to Canada, and which is forced by trends in the tropical Pacific SST. That the historically forced CMIP5 model average does not capture the observed tropical SST pattern further suggests that around half of the recent warming over Canada and Greenland is associated with natural variability that is intrinsic to the coupled atmosphere–ocean system. We note, however, that the observational records in the tropics are temporally and spatially incomplete, and that the simulated response of tropical SSTs to anthropogenic forcing is strongly model-dependent[28]. Hence we cannot rule out the possibility that the pattern of the observed tropical Pacific SST trend may also be associated with external forcing.

METHODS SUMMARY

We used atmospheric circulation and temperature data from the 1979–2013 ERA-interim reanalysis[19], SST data from ERSSTv3 (ref. 29), and sea-ice data from HADISST[30]. We used output from 40 climate models archived in the CMIP5 database[16] to estimate the climate response to external forcing in the historical record. MCA[26] captured the dominant coupled modes between the Northern Hemisphere Z200 (0–88.5° N) change and tropical SST (20° N to 20° S). We used the ECHAM4.6 (ref. 27) atmospheric general circulation model to simulate the circulation and temperature response forced by the observed tropical (30° N to 30° S) SST trends; in the extratropics, the ECHAM4.6 is coupled to a slab ocean with a simple, thermodynamic-only sea ice model. We focus on the annual average in this study because the recent temperature and circulation changes over the region of interest are similar across all seasons. To construct an annual mean, we averaged the 12 months from June through to the end of the following May. Note that the year label refers to June (for example, the annual mean of 2012 is the average from June 2012 through to the end of May 2013). The results presented in this study are not sensitive to how the annual average is constructed. It should be noted that because the historical record of reliable data for the Northern Hemisphere polar region is short, the term 'trend' used in the main text refers to any low-frequency variability distinct from the inter-annual variability; it does not necessarily imply a long-term trend, but may simply reflect decadal variability.

Online Content Any additional Methods, Extended Data display items and Source Data are available in the online version of the paper; references unique to these sections appear only in the online paper.

Received 19 October 2013; accepted 12 March 2014.

1. Kirtman, B. *et al.* in *Climate Change 2013: The Physical Science Basis* (eds Stocker, T. F. *et al.*) 953–1028 (Cambridge Univ. Press, 2013).
2. Serreze, M. C. & Barry, R. G. Processes and impacts of Arctic amplification: a research synthesis. *Global Planet. Change* **77,** 85–96 (2011).
3. Polyakov, I., Walsh, J. E. & Kwok, R. Recent changes of Arctic multiyear sea ice coverage and the likely causes. *Bull. Am. Meteorol. Soc.* **93,** 145–151 (2012).
4. Serreze, M. C., Barrett, A. P., Stroeve, J. C., Kindig, D. M. & Holland, M. M. The emergence of surface-based Arctic amplification. *Cryosphere* **3,** 11–19 (2009).
5. Screen, J. A. & Simmonds, I. The central role of diminishing sea ice in recent Arctic temperature amplification. *Nature* **464,** 1334–1337 (2010).
6. Chylek, P., Folland, C. K., Lesins, G., Dubey, M. K. & Wang, M. Y. Arctic air temperature change amplification and the Atlantic multidecadal oscillation. *Geophys. Res. Lett.* **36,** L14801 (2009).
7. Graversen, R. G., Mauritsen, T., Tjernstrom, M., Kallen, E. & Svensson, G. Vertical structure of recent Arctic warming. *Nature* **451,** 53–56 (2008).
8. Lee, S. Testing of the tropically excited Arctic warming (TEAM) mechanism with traditional El Nino and La Nina. *J. Clim.* **25,** 4015–4022 (2012).
9. Francis, J. A. & Hunter, E. New insight into the disappearing Arctic sea ice. *Eos* **87,** 509–511 (2006).
10. Abbot, D. S., Walker, C. & Tziperman, E. Can a convective cloud feedback help eliminate winter sea ice at high CO_2 concentration? *J. Clim.* **22,** 5719–5731 (2009).
11. Hansen, J. & Nazarenko, L. Soot climate forcing via snow and ice albedo. *Proc. Natl Acad. Sci. USA* **101,** 423–428 (2004).
12. Shindell, D. & Faluvegi, G. Climate response to regional radiative forcing during the twentieth century. *Nature Geosci.* **2,** 294–300 (2009).
13. Yoo, C., Feldstein, S. & Lee, S. Impact of the Madden-Julian Oscillation trend on the polar amplification of surface air temperature during 1979–2008 boreal winter. *Geophys. Res. Lett.* **38,** L24804 http://dx.doi.org/10.1029/2011GL049881 (2011).
14. Barnston, A. G. & Livezey, R. E. Classification, seasonality and persistence of low-frequency atmospheric circulation patterns. *Mon. Weath. Rev.* **115,** 1083–1126 (1987).
15. Hurrell, J. W. Decadal trends in the North Atlantic Oscillation: regional temperatures and precipitation. *Science* **269,** 676–679 (1995).
16. Taylor, K. E., Stouffer, R. J. & Meehl, G. A. An overview of the CMIP5 and the experimental design. *Bull. Am. Meteorol. Soc.* **93,** 485–498 (2012).
17. Screen, J. A., Deser, C. & Simmonds, I. Local and remote controls on observed Arctic warming. *Geophys. Res. Lett.* **39,** L10709 (2012).
18. Bromwich, D. H., Fogt, R. L., Hodges, K. I. & Walsh, J. E. A tropospheric assessment of the ERA-40, NCEP, and JRA-25 global reanalyses in the polar regions. *J. Geophys. Res.* **112,** D10111 (2007).
19. Dee, D. P. *et al.* The ERA-Interim reanalysis: configuration and performance of the data assimilation system. *Q. J. R. Meteorol. Soc.* **137,** 553–597 (2011).
20. Rienecker, M. M. *et al.* MERRA: NASA's modern-era retrospective analysis for research and applications. *J. Clim.* **24,** 3624–3648 (2011).
21. Willmott, C. J. & Matsuura, K. Smart interpolation of annually averaged air temperature in the United States. *J. Appl. Meteorol.* **34,** 2577–2586 (1995).
22. Hansen, J., Ruedy, R., Sato, M. & Lo, K. Global surface temperature change. *Rev. Geophys.* **48,** RG4004 (2010).
23. Hurrell, J. W. & Deser, C. North Atlantic climate variability: the role of the North Atlantic Oscillation. *J. Mar. Syst.* **78,** 28–41 (2009).
24. Hoerling, M. P., Hurrell, J. W. & Xu, T. Y. Tropical origins for recent North Atlantic climate change. *Science* **292,** 90–92 (2001).
25. Graf, H.-F. & Zanchettin, D. Central Pacific El Niño, the "subtropical bridge," and Eurasian climate. *J. Geophys. Res.* **117,** D01102 (2012).
26. Wallace, J. M., Smith, C. & Bretherton, C. S. Singular value decomposition of wintertime sea surface temperature and 500-mb height anomalies. *J. Clim.* **5,** 561–576 (1992).
27. Roeckner, E. *et al. The Atmospheric General Circulation Model ECHAM-4: Model Description and Simulation of Present-Day Climate* (Max Planck Institut für Meteorologie Report 218, 1996).
28. Guilyardi, E. *et al.* New strategies for evaluating ENSO processes in climate models. *Bull. Amer. Meteorol Soc.* **93,** 235–238 (2012).
29. Smith, T. M., Reynolds, R. W., Peterson, T. C. & Lawrimore, J. Improvements to NOAA's historical merged land-ocean surface temperature analysis (1880–2006). *J. Clim.* **21,** 2283–2296 (2008).
30. Rayner, N. A. *et al.* (2003) Global analyses of sea surface temperature, sea ice, and night marine air temperature since the late nineteenth century. *J. Geophys. Res.* **108**(D14), 4407, http://dx.doi.org/10.1029/2002JD002670 (2003).

Acknowledgements We thank the Max Planck Institute for Meteorology model developer for making ECHAM4.6 available and C. Bitz, Q. Fu, D. L. Hartmann, D. Frierson and W.-J. Li for discussion. This work was supported by the US National Science Foundation (OPP 1043092 and ATM 1122989). Q.D. acknowledges support from the University of Washington's Quaternary Research Center and the National Basic Research Program of China (973 Program-2013CB430203). H.-J.K. acknowledges support from the APEC Climate Center.

Author Contributions Q.D. made the calculations, implemented the general circulation model experiments, created the figures, and led the writing of the paper. All authors contributed to the experimental design, and to writing the paper.

Author Information Reprints and permissions information is available at www.nature.com/reprints. The authors declare no competing financial interests. Readers are welcome to comment on the online version of the paper. Correspondence and requests for materials should be addressed to Q.D. (qinghua@uw.edu)

METHODS

Data. Atmospheric circulation and temperature data are from the 1979–2013 ERA-Interim reanalysis[19] and the Modern Era Retrospective-Analysis for Research and Applications (MERRA)[20] reanalysis. SST data are from ERSSTv3 (ref. 29). Sea-ice data are from HADISST[30]. Rainfall data are from GPCP[31]. We also use land-only station surface and near-surface temperature data from University of Delaware[21] and NASA GISS Surface Temperature (GISTEMP)[22]. We used output from the historical simulations of 40 climate models (Extended Data Table 1) that are archived in the CMIP5 (ref. 16) database.

MCA. We use maximum covariance analysis (MCA[26]) to capture the dominant coupled modes between the Northern Hemisphere Z200 (0–88.5° N) change and tropical SST (20°N to 20°S). MCA organizes the variance in two data sets into orthogonal patterns that maximize the covariance in the data.

Wave flux analysis. Wave activity analysis[32] is used to reveal stationary Rossby wave energy propagation. The wave flux vector provides direct information on the flux of wave activity, which is parallel to the group velocity of quasi-stationary Rossby waves. This diagnostic tool is well suited for detection of propagating large-scale quasi-stationary Rossby waves.

Climate model. The general circulation model used to perform the experiments in this study is the ECHAM4.6 atmospheric general circulation model[27], at horizontal resolution of T42 (~2.8° latitude × 2.8° longitude) with 19 vertical levels. We coupled the ECHAM4.6 to a slab ocean, whereby the ocean is represented as boxes of water of uniform specified depth (50 m). A simple, thermodynamic-only sea-ice model is included when the ocean temperature reaches the freezing point. The ocean temperature or sea-ice condition at each grid point is affected only by heat exchange across the air–sea interface; there is no direct communication between adjacent ocean grid points, nor is there any representation of the deep ocean. In addition, a cyclostationary climatological heat flux is added to the ocean temperature tendency equation in order to maintain a seasonal cycle of ocean temperature and sea ice condition that is as close to that observed.

31. Huffman, G. J., Adler, R. F., Bolvin, D. T. & Gu, G. Improving the global precipitation record: GPCP version 2.1. *Geophys. Res. Lett.* **36,** L17808 (2009).
32. Plumb, R. A. On the three-dimensional propagation of stationary waves. *J. Atmos. Sci.* **42,** 217–229 (1985).

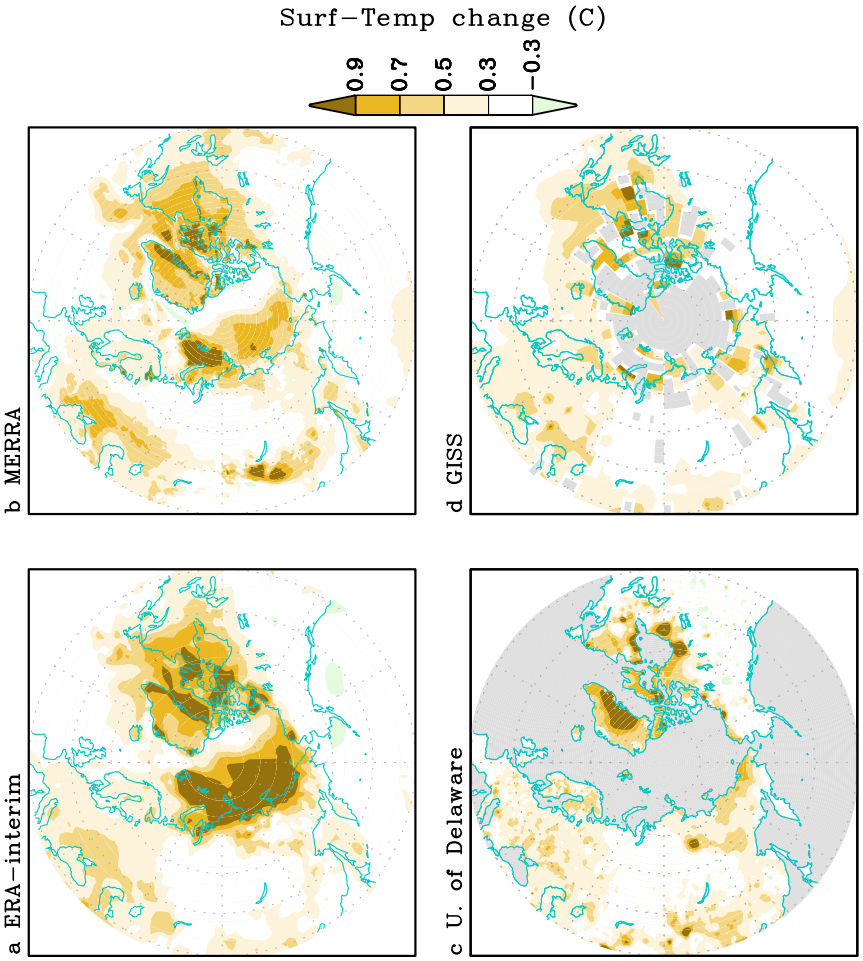

Extended Data Figure 1 | Observed trend pattern of annual mean surface temperature for 1979–2012. Linear trend (per decade) of annual mean surface and near-surface temperature for **a**, ERA-interim, **b**, MERRA reanalysis, **c**, University of Delaware and **d**, GISTEMP for the period of 1979–2012. The grey regions in **c** and **d** indicate no data.

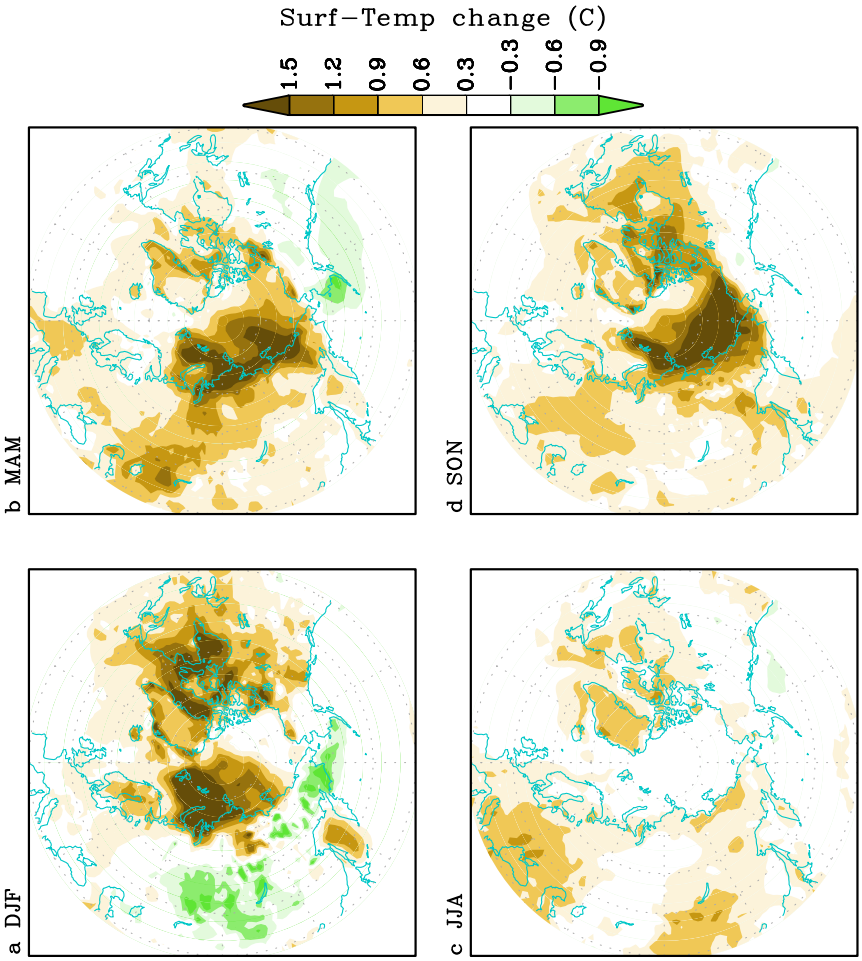

Extended Data Figure 2 | Observed trend pattern of seasonal mean surface temperature for 1979–2012. Linear trend (per decade) of seasonal mean ERA-interim surface temperature for **a**, December to February (DJF), **b**, March to May (MAM), **c**, June to August (JJA) and **d**, September to November (SON) for the period 1979–2012.

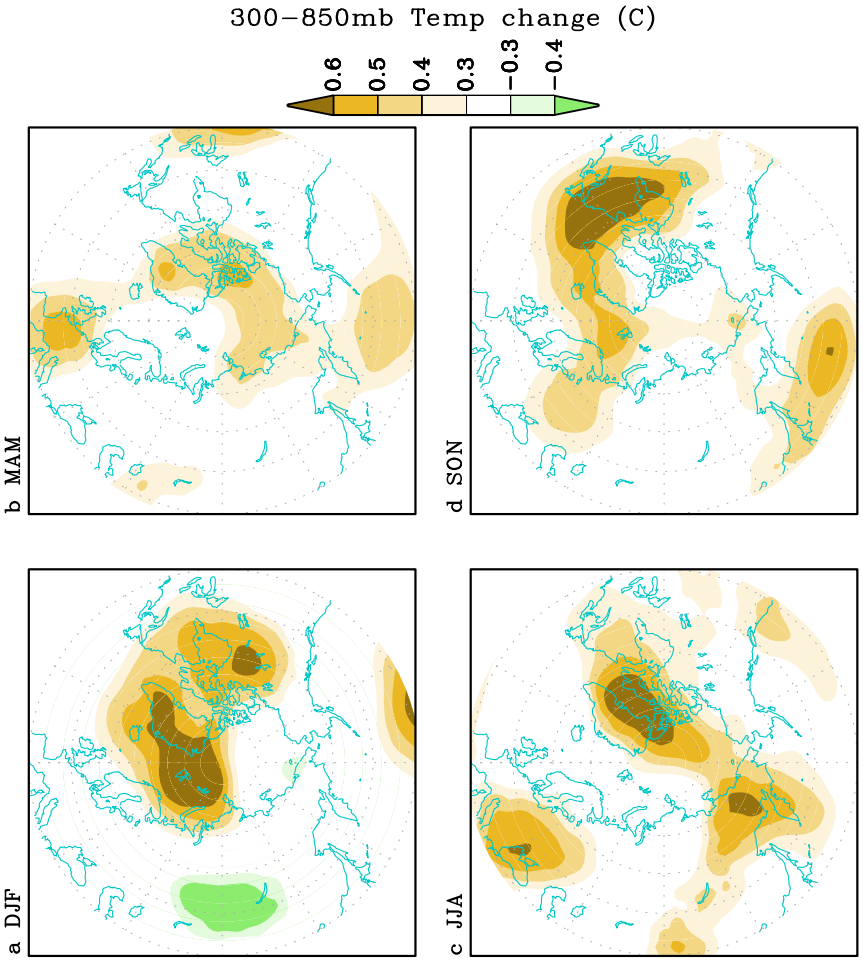

Extended Data Figure 3 | Observed trend pattern of seasonal mean 300–850 hPa temperature for 1979–2012. Linear trend (per decade) of seasonal mean ERA-interim 300–850 hPa temperature for **a**, DJF, **b**, MAM, **c**, JJA and **d**, SON for the period 1979–2012.

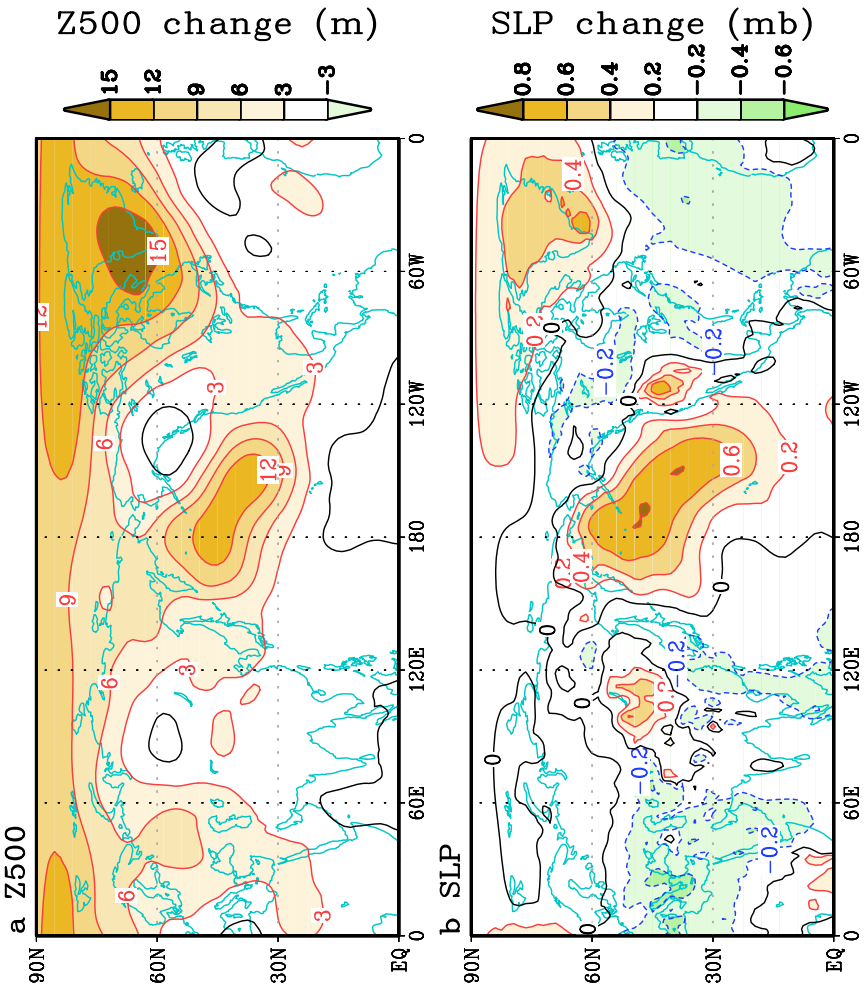

Extended Data Figure 4 | Observed trend pattern of annual mean field for 1979–2012. Linear trend (per decade) of annual mean **a**, 500-hPa geopotential height (Z500), and **b**, sea level pressure (SLP) of ERA-interim for the period 1979–2012. Solid (dashed) contours indicate positive (negative) trends.

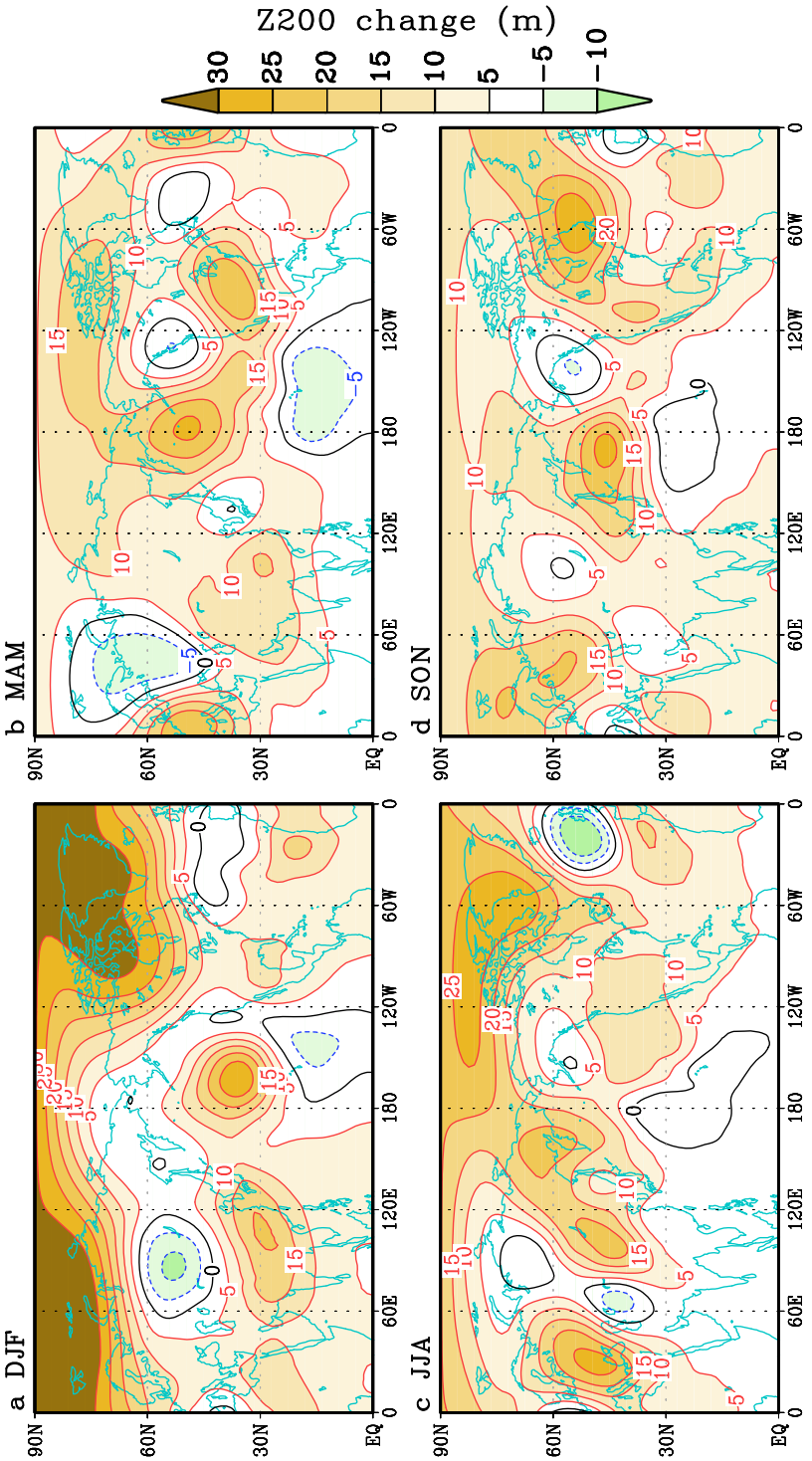

Extended Data Figure 5 | Observed trend pattern of seasonal mean 200-hPa geopotential height for 1979–2012. Linear trend (per decade) of seasonal mean ERA-interim 200-hPa geopotential height for **a**, DJF, **b**, MAM, **c**, JJA and **d**, SON for the period 1979–2012. Solid (dashed) contours indicate positive (negative) trends.

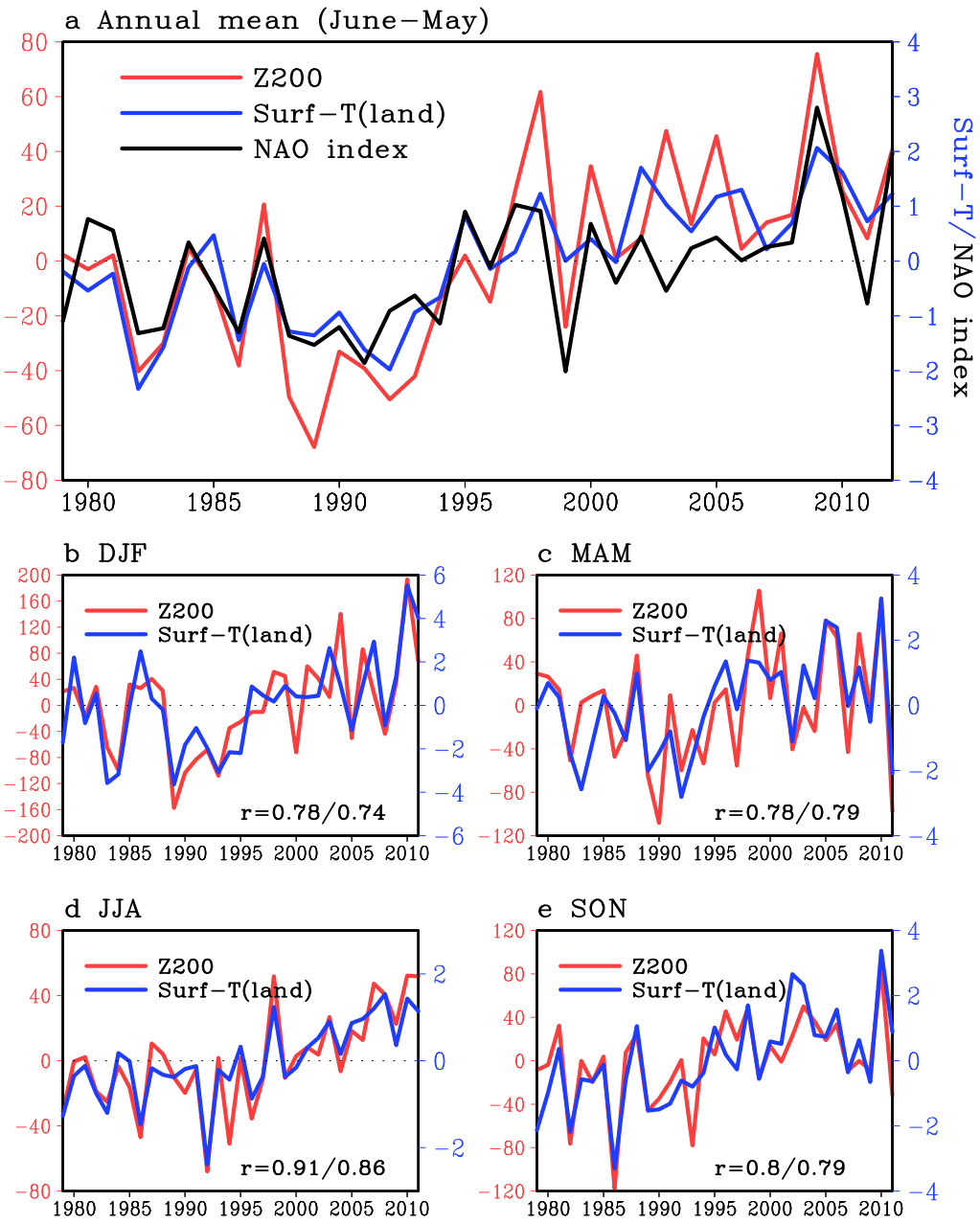

Extended Data Figure 6 | Observed surface temperature and Z200 change in northeastern Canada and Greenland. **a**, Annual mean surface temperature, Surf-T(land), and Z200 averaged over northeastern Canada and Greenland (55° N–85° N, 280° E–340° E, denoted by a box in Fig. 1c), and NOAA NAO index[14] (sign is reversed for simplicity of comparison) for the period 1979–2012. The units on the left ordinate are geopotential metres; the units on the right ordinate are °C (surface temperature) and unitless (NAO index). **b**–**e**, Surface temperature and Z200 averaged over northeastern Canada and Greenland (55° N–85° N, 280° N–340° N, denoted by a box in Fig. 1c) for each season for the period 1979–2012. The correlation coefficient (*r*) of two curves is denoted in the bottom right corner. The first (second) number denotes the correlation between the raw (detrended) time series.

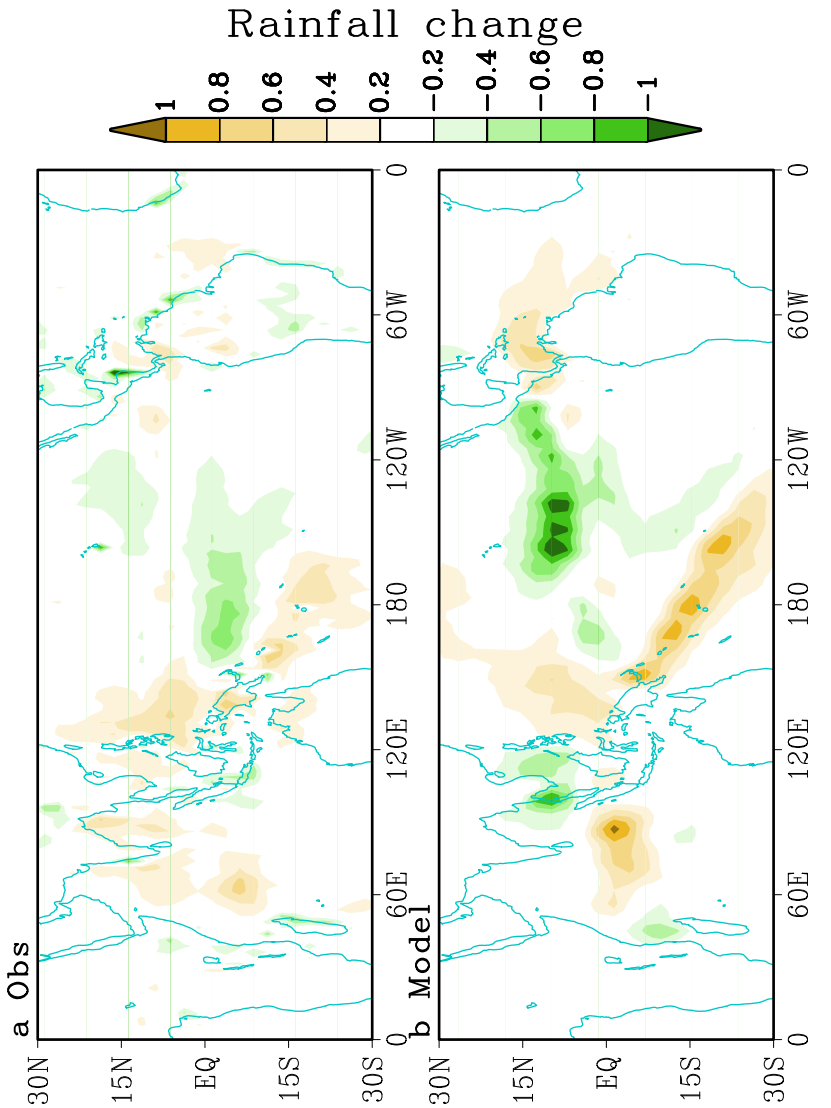

Extended Data Figure 7 | Observed and simulated annual mean tropical rainfall trend patterns for 1979–2012. Linear trend (mm per day per decade) of annual mean **a**, observed GPCP[31] rainfall, **b**, simulated rainfall from 34-year simulation of ECHAM run forced by observed SST (1979–2012) in the tropics (30° N to 30° S). In the extratropics and the polar region, the atmosphere is coupled to a slab ocean model with a thermodynamic sea-ice component.

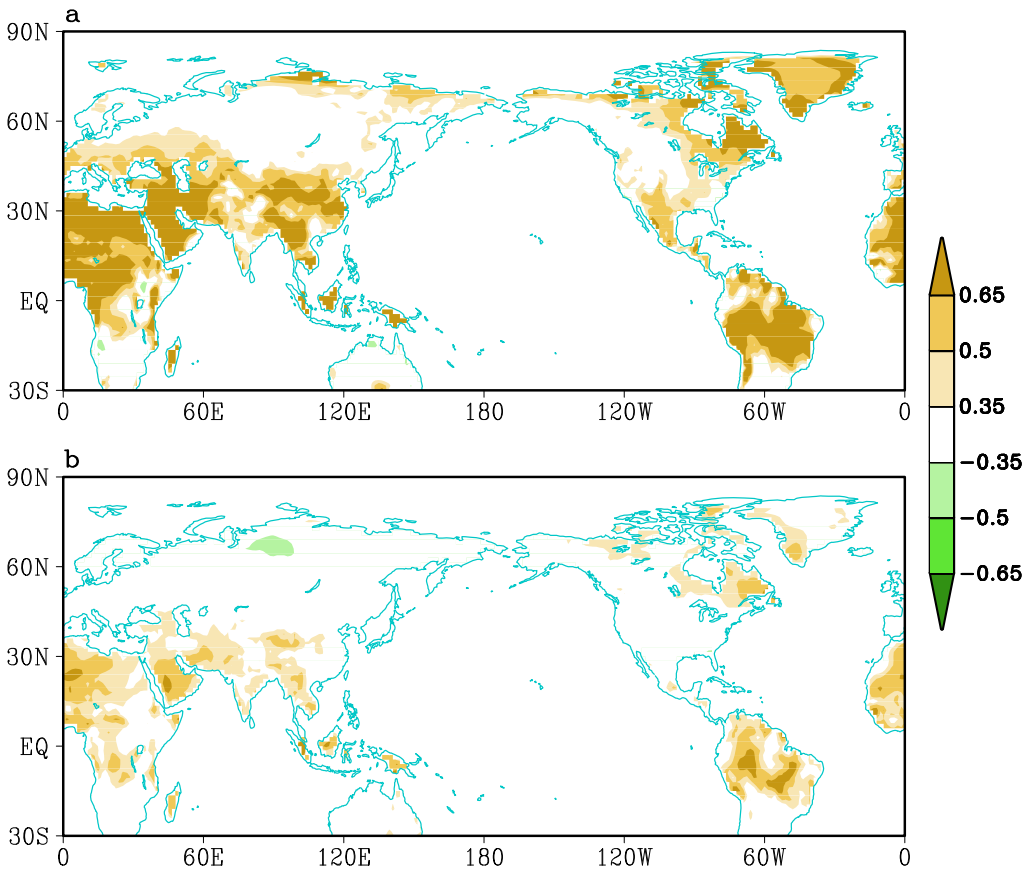

Extended Data Figure 8 | MCA2 SST related annual mean land surface temperature. **a**, Correlation (colour scale shows *r*) between the time series of the MCA2 pattern of annual mean SST (blue curve in Fig. 2d) and annual mean land surface temperature in ERA-interim during 1979–2012. **b**, As **a** but using the detrended surface air temperature data and the detrended time series of mode 2 SST.

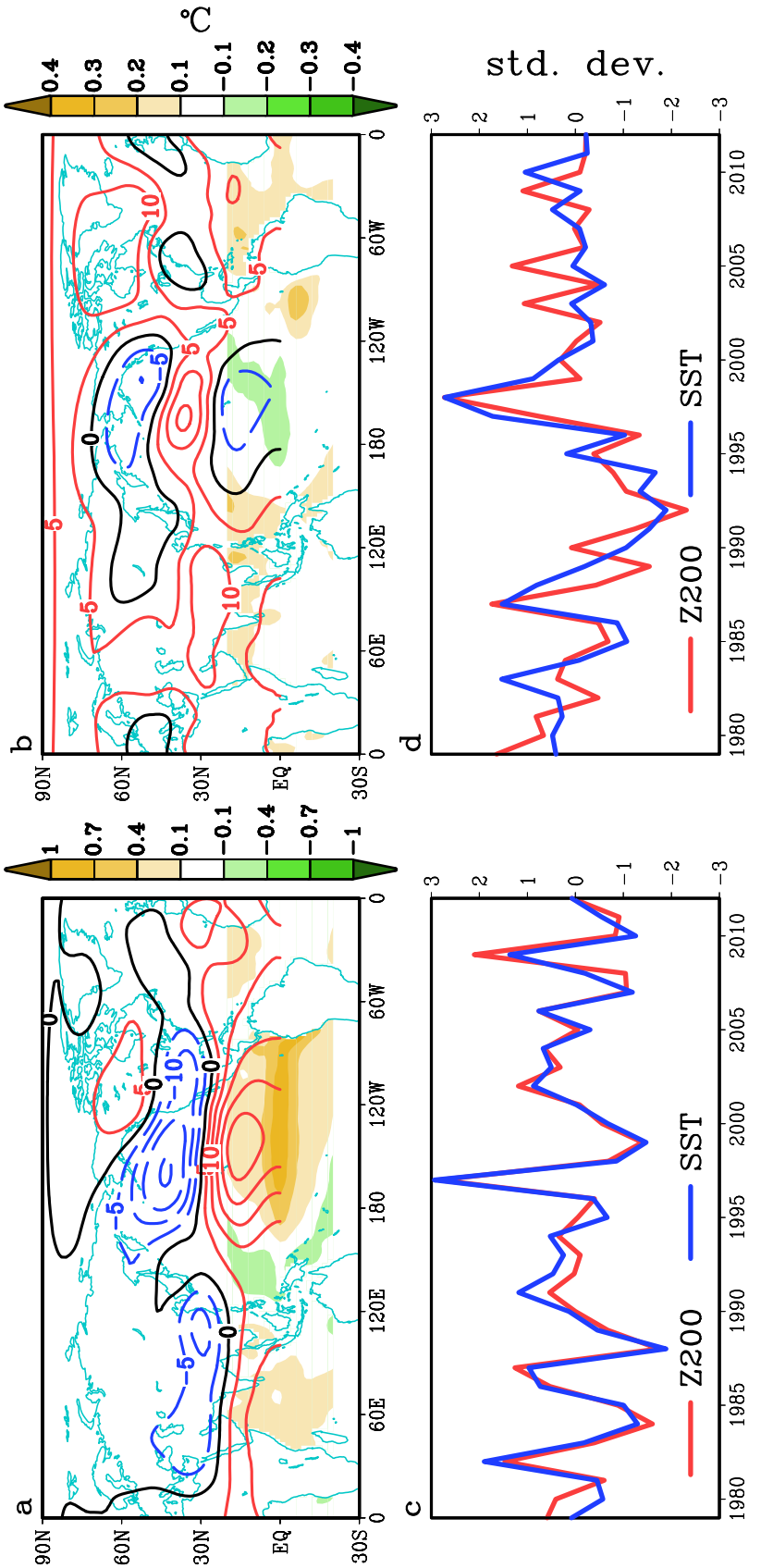

Extended Data Figure 9 | Coupled patterns between detrended annual mean tropical SST and Northern Hemisphere circulation for 1979–2012. Figure shows MCA results for detrended annual mean 1979–2012 Northern Hemisphere (0-88.5° N) 200-hPa geopotential heights (Z200) and tropical (20° S to 20° N) sea surface temperature (SST). Shown in **a** are the patterns of Z200 (contour interval 10 metres) and tropical SST (shading) that accompany the first mode in these two data sets. Panel **c** displays the time series of the Z200 (red) and SST (blue) patterns shown in **a**. Panels **b** and **d** are the same as in **a** and **c** but for the second mode. Amplitudes in **a** and **b** are scaled by one standard deviation of the corresponding time series in **c** and **d**; the latter have a standard deviation of one.

Extended Data Table 1 | 40 climate models in the CMIP5 historical experiment

CMIP5 model designation	nx	ny
1. bcc-csm1-1	128	64
2. bcc-csm1-1-m	320	160
3. CCSM4	288	192
4. CESM1-BGC	288	192
5. CESM1-CAM5	288	192
6. CESM1-FASTCHEM	288	192
7. CESM1-WACCM	144	96
8. CMCC-CESM	96	48
9. CMCC-CM	480	240
10. CMCC-CMS	192	96
11. CNRM-CM5	256	128
12. CSIRO-Mk3-6-0	192	96
13. CanESM2	128	64
14. FGOALS-g2	128	60
15. FGOALS-s2	128	108
16. FIO-ESM	128	64
17. GFDL-CM2p1	144	90
18. GFDL-CM3	144	90
19. GFDL-ESM2G	144	90
20. GFDL-ESM2M	144	90
21. GISS-E2-H	144	89
22. GISS-E2-H-CC	144	89
23. GISS-E2-R	144	89
24. GISS-E2-R-CC	144	89
25. HadCM3	96	73
26. HadGEM2-AO	192	144
27. inmcm4	180	120
28. IPSL-CM5A-LR	96	96
29. IPSL-CM5A-MR	144	143
30. IPSL-CM5B-LR	96	96
31. MIROC-ESM	128	64
32. MIROC-ESM-CHEM	128	64
33. MIROC4h	640	320
34. MIROC5	256	128
35. MPI-ESM-LR	192	96
36. MPI-ESM-MR	192	96
37. MPI-ESM-P	192	96
38. MRI-CGCM3	320	160
39. NorESM1-M	144	96
40. NorESM1-ME	144	96

List of 40 CMIP5 CGCMs used in Fig. 4 to examine the forced response of the climate system to anthropogenic and natural external forcing, along with the number of atmospheric horizontal grids.

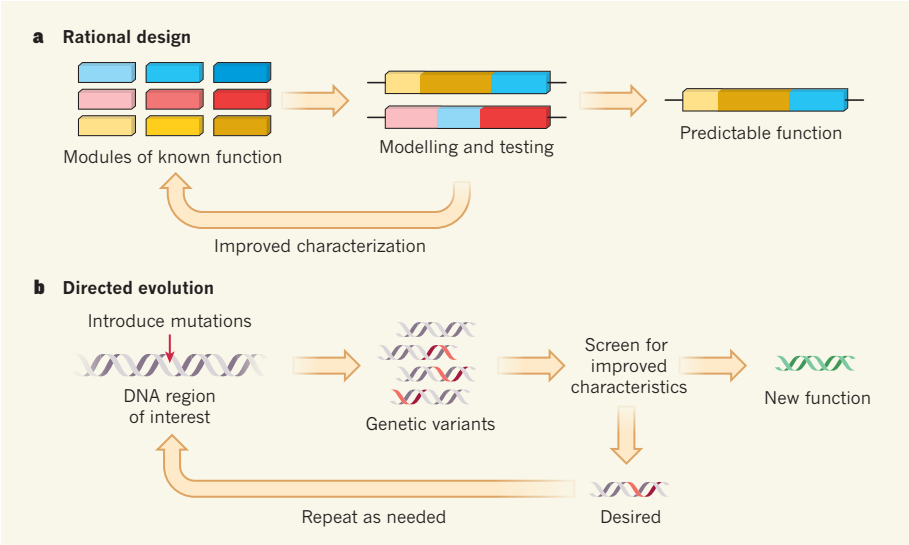

Figure 1 | Two methods for the synthetic engineering of organisms. **a**, In rational design, biological 'parts' (such as genes, gene regulators and proteins) are studied through modelling and testing such that their behaviour is understood. This produces libraries of well-characterized parts — or modules consisting of multiple parts — that can be rationally assembled in cells in different combinations, resulting in predictable functions. **b**, An alternative approach is to harness the power of evolution to direct the design of synthetic organisms. A region of interest (in this example, a gene) is randomly mutated, producing cells that harbour a variety of mutations. The cells are then screened to find those with mutations that result in or improve a desired function. Cells that do not harbour such mutations are eliminated from the pool; those that do can be cultured and then subjected to new rounds of mutation and screening, to achieve a desired end product.

pathway that compares favourably with nature's engineering outputs. Nature's writing is intricate (some say convoluted and opaque), but it is effective. We are just learning to hold the pencil.

The reason is simple: in biology, details matter a lot, and we don't understand the details. Rational design is hard when one cannot even predict the effects of a single mutation in a single enzyme, or the full impact of adding a single gene to the thousands already present in an organism. It is fine to hope that 'modular' biology is possible, but our ham-fisted attempts at assembling biological components usually show that biology is anything but modular. The engineering of systems that tackle real-world problems, such as producing an antimalarial drug or an alternative fuel through a new microbial pathway, involves years of trial and error[3]. Realizing the potential of synthetic biology requires dealing with the details.

Rational design will not move beyond these problems until our understanding of the details of biology has improved dramatically. Luckily, we do not have to wait. Evolution is a time-tested tool for engineering the details, and we can use it in the lab to circumvent our profound ignorance of how sequence encodes function. Accumulating beneficial mutations over multiple generations is a general algorithm for turning a poor copy-and-paste job into effective writing, and it works at all levels of complexity. From creating a DNA-editing enzyme that excises HIV from the host genome[4], to optimizing multi-enzyme biosynthetic pathways[5], directed evolution has produced results with purpose[6].

Evolutionary engineering is not incompatible with 'rational' design; in fact, the two are highly complementary. Directed evolution requires a starting design, and the better the design, the easier the evolution. Evolution also requires a rational search strategy. Where should mutations be targeted, and how many of them? How do we measure success along the way? Directed evolution and rational design are even claiming common ground, for example in mutant libraries that have been designed with input from computational processes, accelerating the evolutionary process[7].

With a good starting point in hand, evolution is the most direct approach to engineering the biological world, and it is uniquely effective with biological substrates, the products of that same process. Biology is highly evolvable, and we should exploit that feature to the fullest, as we have for thousands of years with everything from rats to racehorses. The writer's best friend is a good editor — the synthetic biologist's should be directed evolution. ■

Frances H. Arnold *and* **Joseph T. Meyerowitz**
are in the Division of Chemistry and Chemical Engineering, California Institute of Technology, Pasadena, California 91125, USA.
e-mails: frances@cheme.caltech.edu; jmeyerow@caltech.edu

1. Gardner, T. S., Cantor, C. R. & Collins, J. J. *Nature* **403,** 339–342 (2000).
2. Kotula, J. W. *et al. Proc. Natl Acad. Sci. USA* http://dx.doi.org/10.1073/pnas.1321321111 (2014).
3. Keasling, J. D. *Proc. Am. Phil. Soc.* **156,** 283–294 (2012).
4. Sarkar, I., Hauber, I., Hauber, J. & Buchholz, F. *Science* **316,** 1912–1915 (2007).
5. Bastian, S. *et al. Metab. Eng.* **13,** 345–352 (2011).
6. Romero, P. A. & Arnold, F. H. *Nature Rev. Mol. Cell Biol.* **10,** 866–876 (2009).
7. Trudeau, D. L., Smith, M. A. & Arnold, F. H. *Curr. Opin. Chem. Biol.* **17,** 902–909 (2013).

CLIMATE SCIENCE

The origin of regional Arctic warming

Observational data and modelling show that the rapid warming of the northeastern Canada and Greenland sector of the Arctic over the past three decades has been strongly driven by cooling in the tropical Pacific Ocean. SEE LETTER P.209

JÜRGEN BADER

Over the past 30 years, Earth has become a warmer place. One of the most striking examples of surface-temperature warming is the polar regions in the Northern Hemisphere (Fig. 1). The greater warming in the Arctic[1], compared with the global mean, is associated with a reduction in sea ice[2] and dynamical and radiative feedbacks[3], and is widely attributed to anthropogenic climate change. But the fact that the warming is not spatially uniform raises the question of whether natural climate variability has a role in driving it and causing regional climate change. On page 209 of this issue, Ding *et al.*[4] show that the most prominent Arctic warming has occurred in northeastern Canada and Greenland, and that cooling in the tropical Pacific Ocean forced half of the warming in these two regions. The findings indicate that a substantial part of regional Arctic climate change is therefore a result of natural climate variability.

Much of the interannual and decadal variability in atmospheric climate can be described by the evolution of the leading modes of climate variability, such as the North Atlantic Oscillation (NAO). The NAO consists

of variations in the difference of sea-level atmospheric pressure between the Icelandic low-pressure system (Icelandic low) and the Azores high-pressure system (Azores high), and is most pronounced during boreal winter. In the positive phase of the NAO, there is a considerable difference in pressure between these two systems, with both the Icelandic low and the Azores high being intensified. In the negative phase, the two pressure zones are weakened and the difference between them is less.

The NAO is linked to changes in the intensity and location of the North Atlantic jet stream and storm track, and to large-scale temperature and precipitation variations over Europe, Greenland and North America. It is an intrinsic atmospheric phenomenon, but fluctuations in sea surface temperature (SST) can also affect it. In fact, it can be influenced by both variations in local North Atlantic SST and remote SST in the tropics[5]. Changes in tropical SSTs lead to changes in convection throughout the lowest portion of the atmosphere (the troposphere) at low latitudes, which in turn excite large-scale atmospheric waves called Rossby waves. These waves can propagate to mid- and high latitudes and affect the NAO.

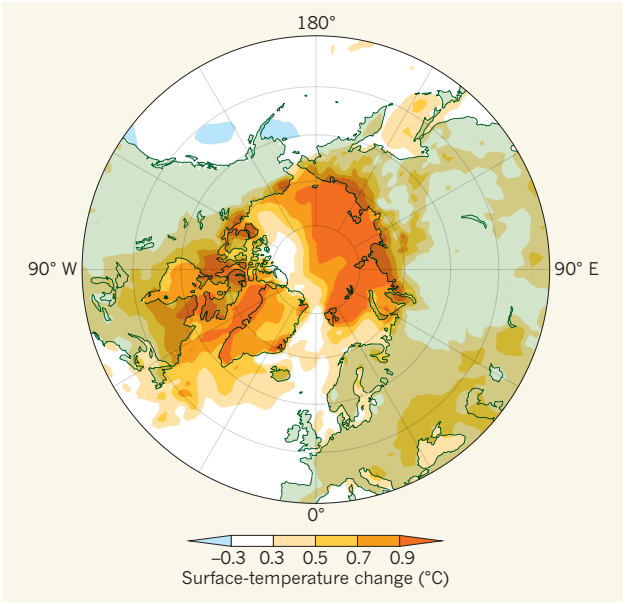

Figure 1 | Trend in annual mean surface temperature. The graphic shows the observed change per decade of annual mean surface and near-surface temperature for the period 1979–2012, based on the ERA-interim climate data set. The most marked warming has occurred in northeastern Canada, Greenland and north Siberia. (Adapted from Extended Data Fig. 1 of ref. 4.)

In their study, Ding *et al.* demonstrate that Rossby waves and the NAO are involved in regional Arctic warming. Their finding that the Arctic warming in northeastern Canada and Greenland since 1979 is strongly driven by cooling in the tropical Pacific is supported by observational data indicating that warming in these two regions is not limited to the surface but also extends to the upper troposphere. The authors argue that it is unlikely that decadal temperature changes in the upper Arctic troposphere are locally forced by variations in surface temperature. They suggest instead that warming at the surface and in the troposphere are the result of atmospheric-circulation changes in the high troposphere, and that these changes are remotely forced. Specifically, Ding *et al.* show that the recent warming in northeastern Canada and Greenland is associated with a negative NAO phase driven by Rossby-wave activity caused by SST cooling in the tropical Pacific.

These results are confirmed by modelling experiments. The authors demonstrate that an atmospheric general circulation model forced by the observed tropical SST can simulate the connection between tropical Pacific SST cooling and regional Arctic tropospheric warming. However, they also show that coupled ocean–atmosphere climate models used in the fifth assessment report of the Intergovernmental Panel on Climate Change fail to reproduce the observed regional pattern of Arctic warming. Two plausible reasons for this failure are worth mentioning. First, the recent cooling in the tropical Pacific can probably be attributed to intrinsic variability of the climate system[6], because it is not simulated by coupled climate simulations that incorporate observed changes in the concentration of greenhouse gases and aerosols. Second, despite continued improvements to climate models, it is still a challenge to simulate the influence of remote climatic phenomena correctly.

By linking cooling in the tropical Pacific with trends in atmospheric circulation and regional Arctic warming, Ding and colleagues highlight the complexity of processes involved in regional climate change. Even remote climatic fluctuations can have a substantial impact. Improving the representation of such teleconnections in climate models should therefore remain a high priority for climate scientists. The authors also note the importance of natural internal climate variability for present and near-future regional Arctic climate. But as greenhouse-gas concentrations are likely to increase in the future, it is only a question of time before external forcing dominates regional Arctic warming. ■

Jürgen Bader *is at the Max Planck Institute for Meteorology, 20146 Hamburg, Germany, and at Uni Climate, Uni Research & the Bjerknes Centre for Climate Research, Bergen, Norway.*
e-mail: juergen.bader@mpimet.mpg.de

1. Graversen, R. G., Mauritsen, T., Tjernström, M., Källén, E. & Svensson, G. *Nature* **451,** 53–56 (2008).
2. Screen, J. A. & Simmonds, I. *Nature* **464,** 1334–1337 (2010).
3. Shindell, D. & Faluvegi, G. *Nature Geosci.* **2,** 294–300 (2009).
4. Ding, Q. *et al. Nature* **509,** 209–212 (2014).
5. Hoerling, M. P., Hurrell, J. W. & Xu, T. *Science* **292,** 90–92 (2001).
6. Kosaka, Y. & Xie, S.-P. *Nature* **501,** 403–407 (2013).

SYNTHETIC BIOLOGY

Construction of a yeast chromosome

One aim of synthetic biology is to generate complex synthetic organisms. Now, a stage in this process has been achieved in yeast cells — an entire yeast chromosome has been converted to a synthetic sequence in a stepwise manner.

DANIEL G. GIBSON & J. CRAIG VENTER

A biological cell is much like a computer — the genome can be thought of as the software that encodes the cell's instructions, and the cellular machinery as the hardware that interprets and runs the software. Advances in DNA technology have made it possible for scientists to act as biological 'software engineers', programming new biological 'operating systems' into cells. Indeed, in 2010, the entire genome of the bacterium *Mycoplasma mycoides* was replaced with a rewritten synthetic genome, generating the first synthetic cell[1]. Now, in a paper published in *Science*, Annaluru *et al.*[2] describe how they have begun rewriting the genome of a more complex organism, that of the yeast species *Saccharomyces cerevisiae*. The researchers report the design and generation of a functional, synthetic chromosome in this yeast, a milestone that they have